Research Square

Preprints are preliminary reports that have not undergone peer review.
They should not be considered conclusive, used to inform clinical practice,
or referenced by the media as validated information.

Enhancing the Sensitivity of Covalent Organic Frameworks for Ciprofloxacin Detection through Strategic Heteroatom Doping (X = N, P, S, Si)

Okpanachi Nuhu Oyibo
nuhu.oyibo.pg89433@unn.edu.ng
University of Nigeria
Lubem Aondoakaa
University of Calabar
Maryann A. Odume
University of Calabar
Jovita K. Ngene
Ebonyi State University

Research Article

Keywords: COF, DFT, Pharmaceutical pollutant, Ciprofloxacin, Adsorption

Posted Date: April 30th, 2026

DOI: https://doi.org/10.21203/rs.3.rs-9324385/v1

License: This work is licensed under a Creative Commons Attribution 4.0 International License.
Read Full License

Additional Declarations: No competing interests reported.

Enhancing the Sensitivity of Covalent Organic Frameworks for Ciprofloxacin Detection through Strategic Heteroatom Doping (X = N, P, S, Si)

Okpanachi Nuhu Oyibo [a*], Lubem Aondoakaa[b], Maryann A. Odume[b], and Jovita K. Ngene[c]

[a] Department of Biochemistry, Faculty of Biological Sciences, University of Nigeria, Nsukka

[b] Department of Chemistry, Faculty of Physical Sciences, University of Calabar, Calabar, Nigeria

[c] Department of Microbiology, Ebonyi State University, Nigeria

Corresponding author email: nuhu.oyibo.pg89433@unn.edu.ng

Abstract

Ciprofloxacin water pollution from poor waste management poses serious ecological and public health risks. In this research, we investigated the adsorption capacity of covalent organic frameworks (COFs) doped with heteroatoms such as nitrogen, phosphorus, sulfur, and silicon to enhance their ability to adsorb ciprofloxacin. Using density functional theory (DFT) with the ωB97XD/6-311G(d) level of theory. This study included structural analysis, electronic properties, spectral analysis, topological studies, and adsorption energy investigations to provide a comprehensive understanding of the COF-ciprofloxacin interaction. The results revealed that the bare COF was strongly chemisorbed with ciprofloxacin, with an adsorption energy of -1.088 eV. Conversely, doping COFs with nitrogen alone or in combination with sulfur and silicon significantly improved chemisorption, with adsorption energies of -1.116 eV, (N-COF-CFN) -1.415 eV, (N-COF-S-CFN), and -1.687 eV (N-COF-Si-CFN). These findings suggest that specific heteroatom doping can significantly enhance the adsorption capacity of COF for ciprofloxacin.

Keywords: *COF, DFT, Pharmaceutical pollutant, Ciprofloxacin, Adsorption*

1.0 Introduction

The environment is essential for sustaining life on Earth, providing clean air, water, and food. However, human actions have resulted in various environmental problems, such as pollution, deforestation, and climate change. These issues not only impact the environment but also have significant effects on the human body system **[1-3]**. A significant challenge posed by environmental degradation is the presence of pharmaceuticals in water sources **[4-6]**. Ciprofloxacin, a commonly prescribed and broad-spectrum antibiotic, has been found to contaminate water bodies due to improper disposal and inadequate water treatment processes **[7, 8]**. The environmental impact of ciprofloxacin as a pollutant is substantial and has raised concerns about its potential effects on ecosystems and human health. Studies have shown that ciprofloxacin can adversely affect aquatic organisms, such as fish and algae, by disrupting their physiological functions and reproductive capabilities **[9-11]**. Also, the presence of ciprofloxacin in the environment has been linked to the development of antibiotic-resistant bacteria, posing a significant threat to public health and the effectiveness of antibiotics in treating bacterial infections **[12-14]**. This drug can persist for long periods and is known to accumulate in soil, water, and other ecosystems **[15, 16]**. Furthermore, exposure to ciprofloxacin through contaminated water sources or food products can have adverse health effects on humans, including allergic reactions, gastrointestinal disturbances, and the development of antibiotic-resistant infections **[10, 17]**. Ciprofloxacin can disrupt microbial communities, impact nutrient cycling, and harm sensitive organisms such as fish and amphibians **[18]**. Chronic exposure to low levels of ciprofloxacin has been associated with the development of antibiotic resistance in humans, as well as adverse effects on the gut microbiome and overall health. Although efforts have been made to mitigate this challenge through improved wastewater treatment processes, stricter regulations on antibiotic use, and proper waste disposal, these policies have not fully addressed the total removal of ciprofloxacin; hence, there is a need for the development of simple and rapid sensors for its detection and removal.

Interestingly, nanotechnology has gained recognition in scientific research, especially in the field of material science and engineering due to its exceptional electrical, magnetic, mechanical, optical and structural properties which are useful in various applications such as drug delivery, gas sensing, and heterogeneous catalysis **[19-22]**. Many nanomaterials have been investigated for their ability to adsorb various pollutants due to the inefficiency of conventional methods to address the

complexity and diversity of these pollutants. Carbon-based nanomaterials, metal-organic frameworks, metal oxides, and nanocomposites have been explored as adsorbents and sensors **[23-26]**. For instance, Carbon Nanocones (CNCs) have been used for the detection and adsorption of ciprofloxacin from the environment. The outcome of this study showed that the adsorption of ciprofloxacin is exothermic, spontaneous, and occurs with physisorption, with the adsorption being more effective at lower temperatures. This study also reported a 26% reduction in bandgap upon adsorption of ciprofloxacin, indicating heightened electrical conductivity **[27]**. Similarly, Zhao *et al.* (2022) explored the potential of activated carbon to remove ciprofloxacin from wastewater **[28]**. They reported that activated carbon was effective at adsorbing ciprofloxacin, with higher adsorption capacities observed at lower pH levels. These results indicate that activated carbon could be a viable treatment option for removing ciprofloxacin from wastewater before it is released into the environment. Another study conducted by Ajala *et al.* (2023) investigated the ability of biochar, a carbon-rich material produced from biomass, to adsorb ciprofloxacin from water **[29]**. They reported that biochar was effective at removing ciprofloxacin from water, suggesting that biochar could be used as a potential treatment method for contaminated water sources. Also, Han *et al.* (2021) investigated the potential for graphene-based materials to adsorb ciprofloxacin from water **[30]**. The results of their investigation suggested that graphene oxide and reduced graphene oxide were effective at removing ciprofloxacin from water, with higher adsorption capacities observed at lower pH values.

Covalent organic frameworks (COFs) are an intriguing class of crystalline organic polymers built by predesigned building blocks that are linked by strong covalent bonds **[31]**. Unlike the carbon-based and metal oxides materials which often suffer from limited structural modification and poor selectivity, COFs exhibit heightened selectivity, crystallinity, high surface area and modifiable one-dimensional pores making them ideal matrix for biological and chemical sensing Due to these characteristics, COFs have garnered interest and have applied in several fields of material science such as catalysis, energy storage, gas storage, proton conductivity and as solar cells **[32-35]**. Previous studies have also reported on the use of COFs as sensors. For instance, Hussain *et al*. (2020 investigated the sensing potential of luminescent COF for the detection of an indoor pollutant, formaldehyde, using the time-dependent density functional theory method. Their findings revealed the importance of excited-state interaction in determining the sensing behavior of COFs **[36]**. Similarly, Zhu *et al*. worked on the design and synthesis of fluorescent heteropore

COF for the detection of 2,4,6-trinitrophenol (TNP). Here, two COFs with dual pore systems of varying sizes and geometries were prepared that offer hierarchical porosity, which increases diffusion of the analytes and host-guest interactions. These frameworks showed high intrinsic fluorescence, which could be quenched effectively with TNP to achieve both spectroscopic and visual sensations with high selectivity for other nitroaromatic compounds. Most importantly, the heteropore architecture enhanced rapid signal response while improving sensitivity through maximization of available recognition sites in the crystal structure **[37]**. Hence, building on previous studies, we doped COFs with heteroatoms such as nitrogen, phosphorus, sulfur, and silicon to achieve excellent adsorption capacity for ciprofloxacin. The modified COF interacted with ciprofloxacin molecules and was studied via a computational approach. Density functional theory (DFT) was employed, which yielded diverse parameters, such as structural analysis and electronic property studies. These parameters provide insight into the chemical reactivity and kinetic stability of the studied systems. Other parameters, such as spectral analysis, topological studies, adsorption energy investigations, and sensor mechanism parameters, were employed. The parameters applied in this research are believed to provide enriching knowledge of the interaction mechanism between the studied surfaces and the adsorbate.

2.0 Methods

2.1 Computational details

Optimization and computational calculations of the bare and doped complexes were carried out employing the Gaussian 16 software package **[38]**. To this end, Kohn-Sham (K-S) density functional theory (DFT) was employed to investigate the efficacy of these surfaces as potential sensors for the detection of ciprofloxacin, taking into consideration their structural, electronic, and adsorption properties. The selection of an appropriate exchange-correlation functional and corresponding basis set is essential in accurately describing the non-covalent interactions governing the analyte and adsorbent. Hence, all structures were optimized at the ωB97XD/6-311G(d) level of theory. This choice of functional is based on its capability to incorporate both empirical dispersion corrections and long-range interactions, allowing accurate modelling of interactions such as hydrogen bonding, π–π stacking, and van der Waals interactions **[39-40]**. Following optimization, the resulting output files were further converted into formatted checkpoint files, using the Multiwfn 3.7 package **[41]** to compute properties relevant to the sensing

mechanism. Geometric optimization of the systems was carried out using Gaussview 6.0.16 software **[42]**, focusing on variations in bond length before and after interaction with the analyte. Additionally, the electronic properties of the complexes were explored by FMO, NBO, and DOS analysis. Visualization of the optimized geometries and HOMO-LUMO plots of all structures was obtained using Chemcraft and ChemDraw **[43-44],** while the DOS plots were obtained using the 2018 Origin software **[45]**. Furthermore, the nature and strength of interactions of the systems were investigated via the Non-Covalent Interaction (NCI) and Quantum Theory of Atom in Molecules (QTAIM) analysis. The visual representation of NCI surfaces was obtained with the Visual Molecular Display (VMD) Software **[46]** while the Multiwfn 3.7 **[41]** package was used to perform the QTAIM analysis. Additionally, the systems were subjected to Ultraviolet Visible (UV-Vis) spectroscopy analysis to obtain mechanistic information on the optical and excitation behavior of the investigated systems on exposure to ultraviolet rays. Lastly, adsorption studies of the proposed adsorbents were computed to determine how they adsorb, sense, interact, and separate from the Ciprofloxacin pollutants.

3.0 Results and discussion

3.1 Geometry optimization

This analysis provides detailed information about the optimized structures of the various absorbents and the interacting systems (absorbents-absorbates) **[47**, **48]**. The investigated systems were optimized at the ωB97XD/6-311G(d) level of theory, and the respective bond lengths were selected and examined, as shown in **Table 1**. Initially, the complex, COF-CFN, was observed with bond lengths of 1.085 Å, 1.085 Å, and 1.085 Å at the H_{49}–C_{47}, H_{91}–C_{89}, and H_{79}–C_{77} bond labels, respectively. However, upon interaction with CFN, the bond length slightly increased to 1.086 Å, 1.085 Å, and 1.086 Å. In the same vein, N-COF-CFN was observed with 1.415 Å, 1.085 Å, and 1.085 Å before interaction with CFN, whereas, shorter bond lengths were recorded after interactions with bond lengths of 1.413 Å, 1.084 Å, and 1.081 Å corresponding to N102–O1, C_{23}–H_{25}, and C_{19}–H_{21} bonds, respectively, implying that the system is more conjugated after introducing nitrogen. This highlights greater concordance and stability. Going further, N-COF-P-CFN exhibited the following bond lengths: 1.191 Å, 1.383 Å, and 1.554 Å before interaction, and 1.210 Å, 1.353 Å, and 1.570 Å after interaction at the B_{28}–H_{96}, B_2–O_9, and C_{92}–B_{66} labels, respectively. Similarly, the modified N-COF-S surface exhibited a change in bond length after interacting with CFN. The initial lengths recorded at the N_{100}–O_1, S_{102}–O_3, and C_{18}–H_{2O} labels are

1.233 Å, 1.683 Å, and 1.081 Å, respectively. Whereas 1.236 Å, 1.6862 Å, and 1.080 Å lengths were recorded, respectively, after the CFN interaction. Finally, N-COF-Si-CFN has a bond length of 1.431 Å, 1.697 Å, and 1.082 Å before interaction and 1.411 Å, 1.710 Å, and 1.081 Å after interaction at the corresponding bond labels of N_{100}–O_1, Si_{102}–O_1, and C_{18}–H_{20}, respectively. Closely studying the results presented in **Table 1**, it is observed that the interaction of the adsorbent and adsorbate led to the formation of new bonds across all complexes, with recorded higher bond lengths implying the high reactivity tendency of these species.

Table 1. Computed bond length outcomes for the studied systems

System	**Bond label**	**Bond distance (Å)**	
		Before Ads.	**After Ads.**
COF-CFN	H_{49} - C_{47}	1.085	1.087
	H_{91} - C_{89}	1.085	1.086
	H_{79} - C_{77}	1.085	1.086
	H_{52} - O_{104}	-	2.330
	N_{109} - O_{72}	-	3.321
N-COF-CFN	N_{102} - O_1	1.415	1.414
	C_{23} - H_{25}	1.085	1.084
	C_{19} - H_{21}	1.086	1.082
	N_{108} - C_{12}	-	3.836
	O_{31} - F_{103}	-	3.069
N-COF-P-CFN	B_{28} - H_{96}	1.191	1.210
	B_2 - O_9	1.383	1.353
	C_{92} - B_{66}	1.554	1.571
	C_{26} - O_{104}	-	3.167
	P_{102} - F_{103}	-	3.830
N-COF-S-CFN	N_{100} - O_1	1.234	1.236
	S_{102} - O_3	1.684	1.686
	C_{18} - H_{20}	1.082	1.081
	O_{29} - C_{115}	-	3.663
	C_{14} - F_{103}	-	3.194
N-COF-Si-CFN	N_{100} – O_1	1.431	1.412
	Si_{102} – O_1	1.697	1.711
	C_{18} - H_{20}	1.082	1.081
	H_{55}-O_{106}	-	2.890
	Si_{102}-N_{109}	-	3.325

3.2 Vibrational analysis

Vibrational analysis provides insights into the chemical bonds and interactions within sensor materials **[49]**. However, key vibrational modes, such as stretching, wagging, rocking, scissoring, and twisting, are indicative of the molecular structure and functional groups present in materials **[50]**. The provided vibrational analysis results (**Table S1**) for different COF-based systems illustrate various vibrational modes and their corresponding frequency values in cm^{-1}. These modes include symmetric and asymmetric stretching, wagging, rocking, scissoring, twisting, and torsional movements of different molecular groups, such as benzene rings, -C=C, C-C, CH_2, and -C=O. In the COF system, the primary vibrational modes include asymmetric (3194 cm^{-1}) and symmetric (3212 cm^{-1}) stretching of the benzene ring, along with wagging (1696, 1426 cm^{-1}) and rocking (1341 cm^{-1}) movements of the benzene ring. These vibrations indicate the presence of a stable aromatic system within the COF framework **[51]**. The COF-CFN system exhibits symmetric stretching of the C–C bond (3280 cm^{-1}), antisymmetric stretching of the benzene ring (3210 cm^{-1}), and additional modes such as wagging (1680, 1697 cm^{-1}) and scissoring of CH2 (1600 cm^{-1}). The introduction of CFN likely enhances the stability of the benzene ring and the overall framework due to the additional vibrational modes. The N-COF system shows symmetric (-C=C) (3249 cm^{-1}) and antisymmetric (-C=C) (3203 cm^{-1}) stretching, as well as symmetric stretching of the benzene ring (1696 cm^{-1}). Wagging modes at 1440 and 1342 cm^{-1} further contributed to the vibrational profile, indicating that a robust and stable framework was enhanced by nitrogen incorporation. Conversely, in the N-COF-CFN system, symmetric stretching of C-C (3272 cm^{-1}), antisymmetric stretching of benzene (3191 cm^{-1}), and wagging modes (1622, 1620 cm^{-1}) are observed. Additional modes, such as scissoring of CH2 (1530 cm^{-1}) and symmetry (C=O) (3815 cm^{-1}), suggest enhanced stability due to the presence of CFN and nitrogen, which contribute to a more rigid and stable structure. The N-COF-P system displays symmetric stretching of C-C (3258 cm^{-1}), symmetry of the benzene ring (3204 cm^{-1}), and various wagging modes (1688, 1439, and 1223 cm^{-1}). The torsional mode (772 cm^{-1}) indicates the presence of torsional vibration involving the entire system, suggesting a certain degree of flexibility. In the N-COF-P-CFN system, symmetric stretching of C-C (3264, 3211 cm^{-1}), symmetry of the benzene ring (3100 cm^{-1}), and wagging modes (1691, 1447, 1321 cm^{-1}) are observed. The torsional mode (741 cm^{-1}) and

symmetry (C=O) (3471 cm^{-1}) suggest a balance between flexibility and stability due to the incorporation of CFN and phosphorus. The N-COF-S system shows symmetric (-C=C) stretching (3252, 3205, 3180 cm^{-1}), wagging (1677 cm^{-1}), and symmetric stretching of -N=O (1573.67 cm^{-1}). Also, scissoring of the benzene ring (1165 cm^{-1}) and twisting of C_2H_2 (1009.92 cm^{-1}) indicate a stable yet slightly flexible framework. The N-COF-S-CFN system exhibits symmetry (-C=O) (3813 cm^{-1}), symmetric stretching of C-C (3274 cm^{-1}), and symmetry of -C=C (3201 cm^{-1}). Additional modes include symmetric CH_2 (3150 cm^{-1}), scissoring CH2 (1519 cm^{-1}), and wagging CH_2 (1445 cm^{-1}). The presence of these modes indicates a highly stable structure enhanced by CFN and sulfur. The N-COF-Si system displays symmetry (-C=C) (3239 cm^{-1}), symmetry of the benzene ring (3203 cm^{-1}), and various wagging modes (1691, 1568, 1435 cm^{-1}). The torsional mode (684 cm^{-1}) and additional wagging (B-H) modes (848, 912 cm^{-1}) suggest stability with some degree of flexibility due to silicon incorporation. However, the N-COF-Si-CFN system exhibits symmetry (-C=O) (3710, 3811 cm^{-1}), symmetric stretching of C-C (3277 cm^{-1}), symmetric CH2 (3011 cm^{-1}), and scissoring CH2 (1647 cm^{-1}). Wagging CH2 (1548 cm^{-1}) indicates a stable structure with contributions from both CFN and silicon, enhancing the overall rigidity. However, the stability of each system can be inferred from the presence and frequency of vibrational modes. Higher frequency modes, such as those associated with -C=O and -C=C stretching, indicate stronger bonds and greater stability. Systems such as N-COF-CFN and N-COF-S-CFN show high-frequency modes for -C=O and C-C stretching, suggesting enhanced stability. Conversely, systems with more low-frequency modes, such as torsional and twisting modes, indicate more flexibility and potentially less rigidity. Furthermore, systems incorporating CFNs, such as N-COF-CFN and N-COF-S-CFN, exhibit greater stability because of the presence of high-frequency vibrational modes and a variety of stretching and scissoring movements that contribute to a rigid and stable structure. The incorporation of elements such as nitrogen, phosphorus, sulfur, and silicon further enhances structural stability and introduces specific vibrational characteristics that improve the overall robustness of the COF surface.

3.2.1 UV-vis analysis

To gain comprehensive knowledge of electronic behavior in various orbital states, VU-vis analysis was employed. This analysis utilized the ultraviolet (UV) spectrum to measure the wavelength, oscillatory strength, and excitation energy involved in the absorption of UV light by a compound or molecule. The TD-DFT/ωB97XD/6-311G(d) level of theory was applied during the optimization process to study the behavior of electron systems **[52]**. The computed results in **Table 2** demonstrate that the COF-CFN and N-COF-CFN system has strong UV absorption properties. This is explained by the high excitation energies (> 4.00 eV) and short wavelengths, which fall within the 280–315 nm range of the UV spectrum. N-COF-S-CFN and N-COF-Si-CFN also demonstrate promising results, with wavelengths observed within the 315–400 nm spectra. The strong UV absorption demonstrated by these materials is a key indicator of their potential as effective photocatalysts for environmental remediation. The strong UV absorption of these materials shows their promise as photocatalysts for environmental cleanup. Under UV light, they generate reactive species that can break down stubborn pollutants such as ciprofloxacin.

Table 2. UV–Vis results, calculated at the TD-SCF/ωB97XD/6-311++g (d, p) level of theory.

System	Transition Type	Excited State	Excited Energy (eV)	Wavelength (nm)	Oscillator strength (*f*)	Percentage contribution (%)	Transition
COF-CFN	S_0-S_1	323 → 333	4.2836	289.44	0.0007	95	H → L +9
	S_0-S_2	327 → 333	4.4535	278.40	0.1733	121	H → L +5
	S_0-S_3	326 → 335	4.5946	269.85	0.0290	43	H → L +8
N-COF-CFN	S_0-S_1	321 → 333	4.3087	287.76	0.0037	111	H → L +11
	S_0-S_2	328 → 333	4.4225	280.35	0.1783	121	H → L +4
	S_0-S_3	328 → 336	4.5650	271.59	0.0181	88	H → L +7
N-COF-P-CFN	S_0-S_1	333 → 342	0.5178	2394.26	0.0043	85	H → L +8
	S_0-S_2	333 → 335	1.9294	642.61	0.0015	80	H → L +1
	S_0-S_3	333 → 342	2.8244	438.98	0.0042	66	H → L +8
N-COF-S-CFN	S_0-S_1	332A→343A	3.0563	405.67	0.0001	43	H → L +10
	S_0-S_2	317B→334B	3.2764	378.42	0.0051	45	H → L +16
	S_0-S_3	333A→340A	3.2835	377.60	0.0000	57	H → L +6
N-COF-Si-CFN	S_0-S_1	332A→340A	3.3081	374.79	0.0000	89	H → L +7
	S_0-S_2	332A→338A	3.3359	371.67	0.0000	71	H → L +5
	S_0-S_3	333A→335A	3.3452	370.64	0.0092	83	H → L +1

3.3 Electronic properties

3.3.1 HOMO-LUMO analysis

This objective is essential in determining the electronic properties of the systems. The HOMO, which is also known as the highest occupied molecular orbital, is the energy level that is the highest where electrons can be occupied, whereas the LUMO (lowest unoccupied molecular orbital) is the opposite of the HOMO **[53-54]**. An investigation of these orbitals can provide detailed insight into the reactivity and electronic properties of the systems under study. However, one of the key parameters, known as the energy gap, which is the energy variation between the HOMO and LUMO energy levels, is important in determining the reactivity and conductivity of the system. The energy gap was calculated via **equation (1),** and the results are presented in **Table 3**. The contour regions indicating the HOMO and LUMO for each of the systems were captured and are illustrated in **Figure 1a** and **1b**.

$$E_{gap} = \text{LUMO} - \text{HOMO} \qquad (1)$$

The results revealed that the COF had an energy gap of 8.816 eV. Following the doping of N on the COF (N-COF), an energy gap of 8.205 eV was observed. Going further, co-doping the secondary surface with the heteroatoms (P, S, Si) led to a decrease in energy gap with recorded values of 8.207 eV, 7.315 eV, and 7.731eV for N-COF-P, N-COF-S, and N-COF-Si, respectively. Also, the HOMO and LUMO energies of these surfaces were observed to change upon interaction with CFN, resulting in changes in their levels of reactivity and stability. Hence, system COF-CFN has an energy gap of 7.284 eV, arising from the HOMO and LUMO values of -7.857 eV and –0.574 eV. In addition, N-COF-CFN has an energy gap of 7.432 eV, resulting from HOMO and LUMO values of -7.946 eV and -0.514 eV. Similarly, an energy gap of 7.339 eV was observed, with HOMO and LUMO values of -7.739 eV and -0.400 eV, for the N-COF-S-CFN system. Additionally, HOMO and LUMO energies of -7.212 eV and -0.245 eV, were observed for N-COF-P-CFN with a low energy gap of 6.966 eV. Finally, the N-COF-Si-CFN system resulted in the lowest energy gap of 4.601 eV, with corresponding HOMO and LUMO values of -5.795 eV and -1.194 eV, respectively, making it more reactive and less stable. However, these results highlighted the effects of doping heteroatoms and the electronic behavior of the surfaces after interacting with CFN. The surface (COF) has a very high energy gap as a result of a relatively high HOMO energy level, but after doping with heteroatoms, the energy gap decreases, thereby improving its

sensitivity and reactivity characteristics. Interestingly, following the interaction of the surfaces with the CFN molecule, the energy gap was reduced appreciably, suggesting that these surfaces have promising reactivity against CFN; most particularly, the N-COF-P and N-COF-Si surfaces, where energy gaps of 6.966 eV and 4.601 eV were recorded after interacting with CFN.

In addition to accessing the electronic characteristics of these systems using the energy gap, we further investigated the global chemical reactivity descriptors such as hardness (Ƞ), softness (σ), electrophilicity index (ω), chemical potential (μ), and electronegativity (χ), as shown in **Table 3,** to gain wider knowledge of system reactivity and kinetic stability **[55]**. These quantum descriptors were calculated using Koopman's theorem. In these systems, COF and N-COF exhibited the highest chemical hardness values of 4.408 eV and 4.102 eV, respectively; these behaviors remained consistent even after they interacted with the CFN compounds (3.728 and 3.716 eV, respectively), which confirmed the high resistance of the system to deformation and structural rearrangement. Additionally, they were observed with the lowest chemical softness values of 0.113 eV and 0.121 eV, confirming that the systems are less polarized. Notably, the chemical potential results together with the energy gap results indicate that the N-COF-Si-CFN and N-COF-P-CFN systems are highly reactive (-3.495 eV and -3.728 eV) compared with the other systems: N-COF-CFN (-4.230 eV) and N-COF-S-CFN (-4.069 eV). This is ascribed to the change in the chemical potential after the surfaces interact with CFN, wherein the chemical potential of the surfaces initially has highly negative values. Therefore, both the HOMO-LUMO and quantum chemical descriptors suggest that the N-COF-Si and N-COF-P surfaces have very promising sensitivity and chemical reactivity with CFN molecules.

Table 3. HOMO-LUMO and quantum chemical descriptor results evaluated in eV units for the complexes studied

System	HOMO	LUMO	*E*gap	σ	η	μ	ω	χ
COF	-9.257	-0.441	8.816	0.113	4.408	-4.849	2.667	4.849
N-COF	-8.559	-0.354	8.205	0.122	4.103	-4.457	2.421	4.457
N-COF-P	-8.600	-0.393	8.207	0.122	4.104	-4.497	2.464	4.497
N-COF-S	-7.699	-0.384	7.315	0.137	3.658	-4.042	2.233	4.042
N-COF-Si	-8.059	-0.327	7.731	0.129	3.866	-4.193	2.274	4.193
COF-CFN	-7.857	-0.574	7.284	0.137	3.642	-4.215	2.440	4.215
N-COF-CFN	-7.947	-0.515	7.432	0.135	3.716	-4.231	2.409	4.231
N-COF-P-CFN	-7.212	-0.245	6.966	0.144	3.483	-3.729	1.996	3.729
N-COF-S-CFN	-7.739	-0.400	7.339	0.136	3.669	-4.070	2.257	4.070

N-COF-Si-CFN	-5.796	-1.194	4.601	0.217	2.301	-3.495	2.655	3.495

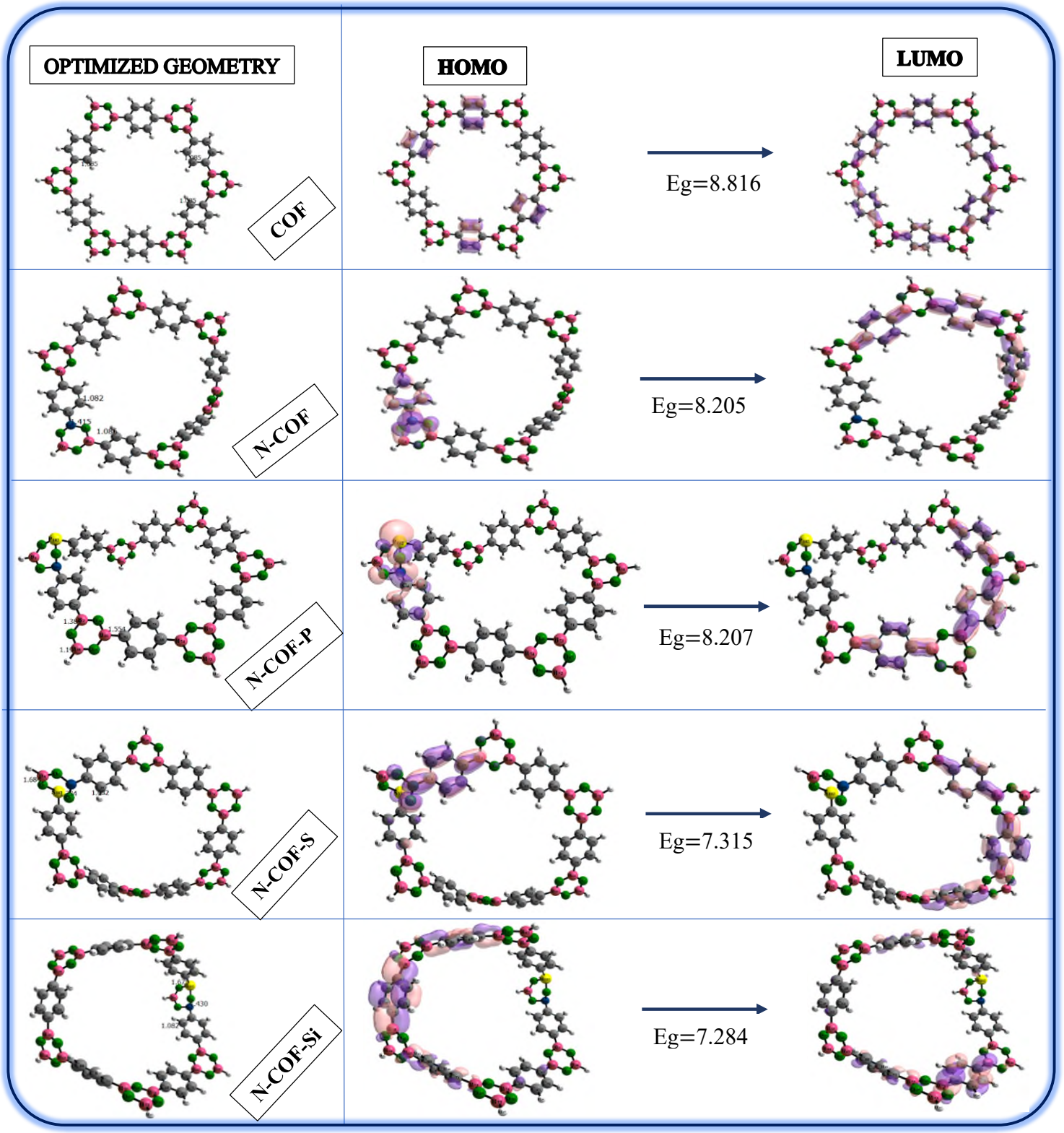


Fig 1a: Demonstration of the HOMO-LUMO regions for the investigated surfaces

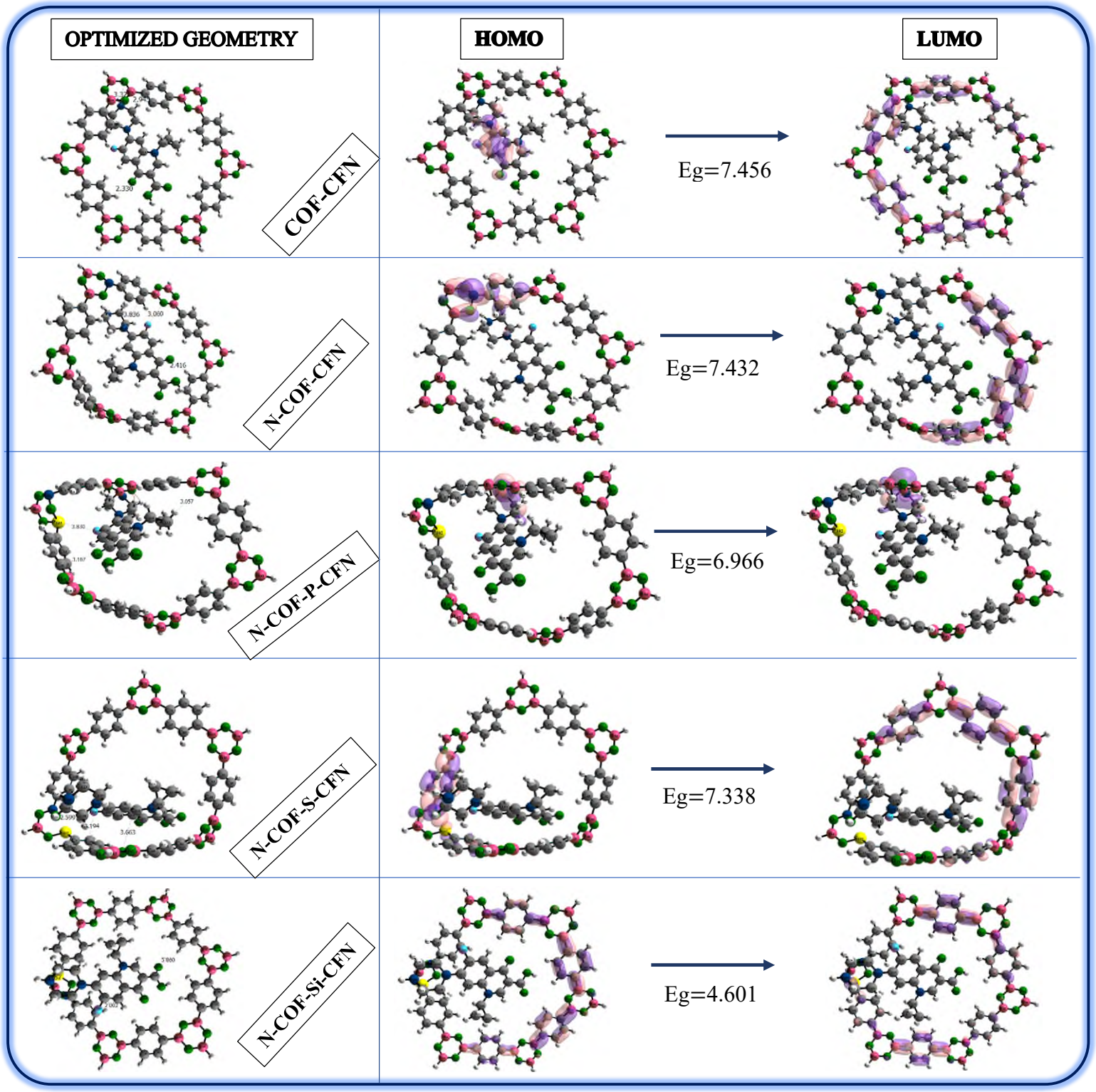


Fig 1b: Demonstration of the HOMO-LUMO regions for the investigated complexes.

3.3.2 Natural bond orbital

This analysis provides vivid information on the transitions of both the donor and acceptor orbitals, providing insights into the intermolecular interactions and charge transfer occurring within the system **[56]**. It also sheds more light on the stability of systems through the perturbation energy and bond transitions that occur during the simulation of a system. Herein, the perturbation energy, also known as the stabilization energy of the studied systems, was computationally determined via **equation 2** as embedded in Gaussian 16 W. During the NBO simulation, other critical parameters were captured, as presented in **Table 4**.

$$E^2 = \Delta E_{i,j} - qi\frac{F^2(i,j)}{Ei-Ej} \qquad (2)$$

where $E^{(2)}$ refers to the second-order perturbation energy, where the value indicates the strength of the interaction. Higher values suggest stronger interactions. E(j)-E(i) is the energy difference between the donor and acceptor orbitals. Smaller values typically indicate a more favorable interaction. F(ij) (Fock matrix element) represents the interaction strength between the donor and acceptor orbitals. Larger values indicate stronger interactions. The results indicate that the COF-CFN system has strong LP → σ* interactions with $E^{(2)}$ values of approximately 100-108 kcal/mol and significant F(ij) values, and the N-COF-CFN system has both LP → σ* and π* → π* interactions, with the latter showing exceptionally high $E^{(2)}$ values, indicating strong π* interactions. The N-COF-S-CFN system displays a mix of π* → π* and LP → σ* interactions with varying strengths. Similarly, the N-COF-Si-CFN system has strong σ → LP* interactions (high F(ij)) and significant π* → π* interactions. Hence, these interactions are essential for understanding the electronic properties and stability of systems.

Table 4. NBO results calculated at DFT/ωB97XD/6-311G(d) level of theory

Systems	Donor (i)	Acceptor (j)	Transition	E^2 Kcal/mol	E(j)-E(i) (a.u)	F(ij) (a.u)
COF-CFN	LP - O_3	σ*O_3 – B_{10}	LP → σ*	106.23	0.89	0.289
	LP – O_6	σ*O_6 - B_{10}	LP→ σ*	108.01	0.88	0.291
	LP – O_{31}	σ*B_5 - O_{31}	LP→ σ*	103.30	0.90	0.086
	LP - O_{67}	σ*B_{30} - O_{67}	LP → σ*	106.43	0.89	0.289

N-COF-CFN	LP - O_{31}	σ^*B_2-O_{31}	LP → σ^*	102.17	0.90	0.285
	π^*C_4-C_{11}	π^*C_{12}-C_{19}	π^*→ π^*	200.06	0.02	0.096
	π^*C_4-C_{11}	π^*C_{20}-C_{28}	π^*→ π^*	331.40	0.01	0.104
	LP-O_{32}	σ^*B_5-O_{32}	LP→ σ^*	115.80	0.66	0.256
N-COF-S-CFN	π^*C_4-C_{10}	π^*C_{11}-C_{18}	π^*→ π^*	163.06	0.01	0.097
	π^*C_7-C_{14}	π^*C_{23}-C_{26}	π^*→ π^*	106.48	0.04	0.116
	LP-O_{67}	σ^*O_{67}-B_{72}	LP→ σ^*	37.60	0.69	0.216
	LP-O_{69}	σ^*O_{69}-B_{73}	LP→ σ^*	38.62	0.65	0.210
N-COF-Si-CFN	π^*C_4-C_{10}	π^*C_{11}-C_{18}	π^*→ π^*	135.71	0.02	0.098
	σ O_3-Si_{102}	LP*-B_8	σ → LP*	173.27	0.68	0.440
	π^*C_7-C_{14}	π^*C_{15}-C_{22}	π^*→ π^*	190.32	0.01	0.097
	π^*C_7-C_{14}	π^*C_{23}-C_{26}	π^*→ π^*	206.87	0.01	0.101

3.3.3 Density of state analysis

Density of state **(**DOS**)** investigations were employed to understand the contributions of various atoms in the studied systems, which play significant roles in the system's reactivity and stability properties since the pristine surface was engineered with other heteroatoms and gained relevant knowledge on the conductivity of the interacting systems. Additionally, this analysis is a crucial tool that can provide more details about the occupation of energy states in line with their respective energy levels **[57]**. Owing to the continuity of energy, as we observed during the HOMO–LUMO analysis, the density of the state of a system can be plotted as a curve **[58]**. In addition, this context provides an understanding of how orbitals are distributed and the strength of each atom fragment within the molecular structure. Therefore, the total density of states (TDOS) outcome can provide insight into the change in the energy gap as it visually transitions to the occupied molecular system. On the other hand, the overlap partial density of states (OPDOS) can offer insight into the determination of bonding, nonbonding, and antibonding orbitals that are involved in the interaction **[59]**. From the results obtained in this study (**Figure 2**), the oxygen and carbon atoms exhibit a unique trend in the HOMO band, whereas the boron and carbon atoms are the dominant contributors of electrons in the LUMO band, indicating their immense contribution to the electronic state for all the surfaces (COF, N-COF, C-COF-P, N-COF-S, and N-COF-Si) and their corresponding interacting complexes (COF-CFN, N-COF-CFN, N-COF-P-CFN, N-COF-S-COF, and N-COFN-Si-CFN). Interestingly, the variations in the HOMO and LUMO energy values

observed earlier are influenced by the presence of heteroatoms doped in the studied adsorbent, as more evidence is seen in the DOS plot, whereby N, P, S, and Si were captured in the HOMO band and LUMO band of the respective surfaces (see **Figure 2**), contributing to their chemical reactivity and kinetic stability potentials. Hence, the Femi energy values for each surface before and after interaction with CFN differ as follows: -10.301 eV, -8.054 eV, -7.949 eV, -6.484 eV, and -6.111 eV, corresponding to the COF, N-COF, N-COF-P, N-COF-S, and N-COF-Si surfaces, respectively. The peaks at -8.355 eV, -8.05 eV, -6.994 eV, -6.506 eV, and -6.172 eV corresponded to the COF-CFN, N-COF-CFN, N-COF-P-CFN, N-COF-S-COF, and N-COFN-Si-CFN complexes, respectively. This demonstrated quick conduction in the N-COF-S and N-COF-Si surfaces even after interaction with the CFN; thus, these surfaces are promising candidates compared with other surfaces.

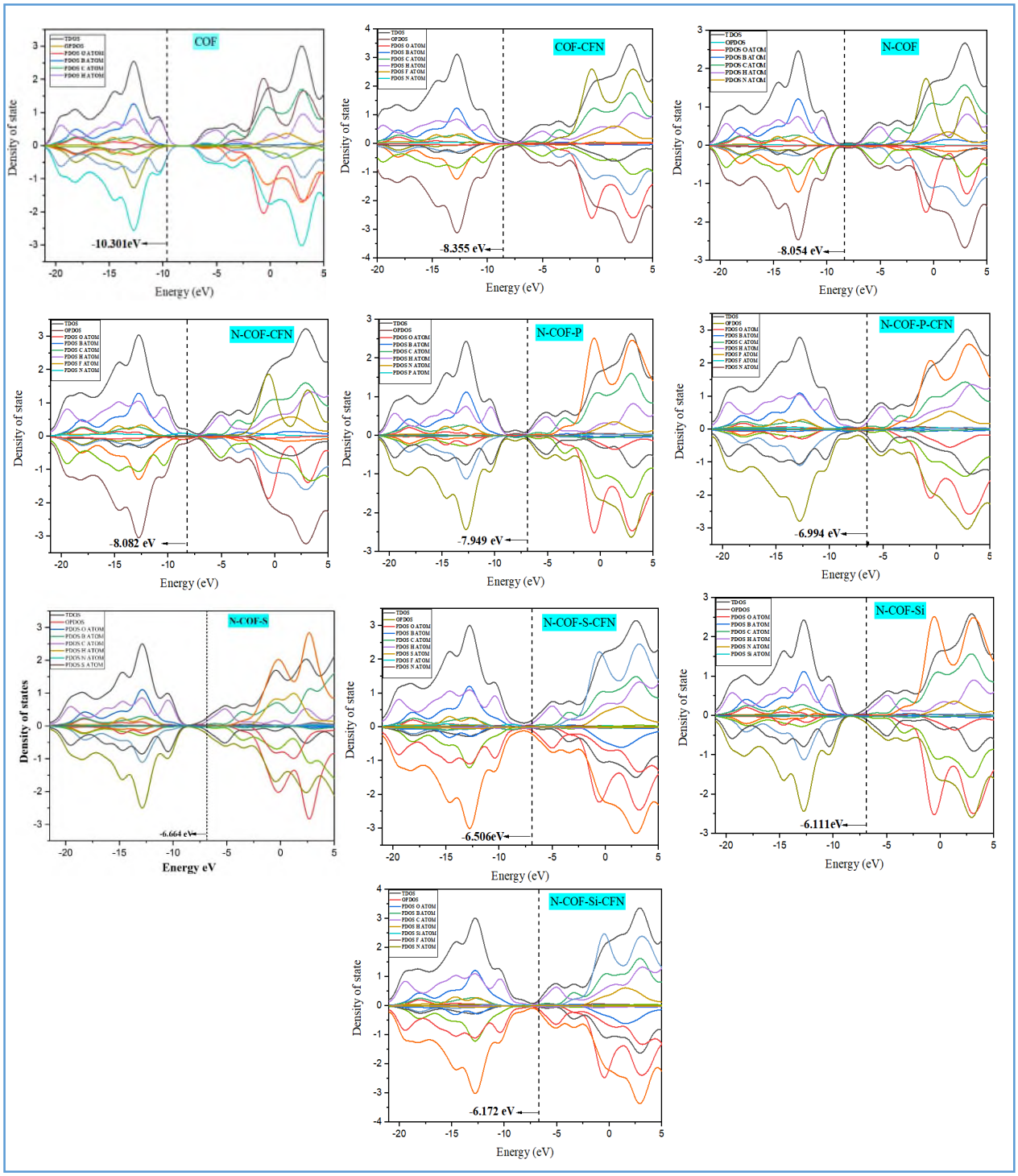


Figure 2. Density of state plot for the investigated systems

3.4.1 Adsorption energy

Adsorption energy is a measure of the energy change when a molecule adsorbs onto a surface **[60]**. Hence, this analysis was employed to gain insight into the adsorption potential of the studied surfaces for ciprofloxacin (CFN). A reported study proposed that a highly negative adsorption energy indicates strong chemisorption, thus indicating a strong interaction between the adsorbate and the adsorbent **[61, 62]**. In the present study, the energy of the systems was obtained on the basis of the applied theoretical method and functions as stipulated in the computational detail, wherein the adsorption energy among the adsorbate–adsorbent complex was possibly determined via **Equation 3 [63]**.

$$E\mathrm{Ads} = E\mathrm{complex} - (E\mathrm{adsorbent} + E\mathrm{adsorbate}) \quad (3)$$

where E_{Ads} is the adsorption energy; $E\mathrm{complex}$ is the energy of the interacting molecules (e.g., COF-CFN); $E\mathrm{adsorbent}$ is the energy of the adsorbent (COF); and $E\mathrm{adsorbate}$ is the energy of the adsorbate (CFN). From the results depicted in **Table 5**, all the surfaces showed chemisorption. The COF without heteroatom incorporation shows better chemisorption than the COFs doped with nitrogen and phosphorus, with energy values of -1.088 eV for COF-CFN and -0.354 eV for N-COF-P-CFN. This implies that the incorporation of combined N and P on the COF surface profoundly affects the adsorption strength of COF, thereby reducing its capacity to adsorb CFN. However, the modification of COFs with N, and upon the combination of S and Si, respectively, improved chemisorption. Thus, N-COF-S-CFN, N-COF-S-CFN, and N-COF-Si-CFN were recorded with corresponding adsorption energies of -1.116 eV, -1.415 eV, and -1.687 eV, respectively. The previous HOMO–LUMO results clearly indicate that combining N and Si enhances the COF reactivity. These two heteroatoms show promising characteristics for strongly enhancing the adsorption of CFN on COF surfaces. In other words, N-COF-Si-CFN has the greatest increase in adsorption strength, making it the most suitable co-dopant among the surfaces studied for enhancing chemisorption **[63-64]**. Therefore, this study reveals that the choice of dopant can significantly influence the adsorption properties of COFs. Sulfur and silicon dopants are particularly effective at increasing the adsorption strength, whereas phosphorus appears to weaken it. This information is critical for designing COFs with tailored adsorption properties for the application of CFN adsorption.

Table 5. Calculated Eads, BSSE corrected, and dipole moment for the studied complexes

Systems	**E_{ads} (eV)**	***E*Ads+BSSE**	**μ (Debye)**
COF-CFN	-1.088	-1.078	7.29
N-COF-CFN	-1.116	-1.106	9.15
N-COF-P-CFN	-0.354	-0.330	7.06
N-COF-S-CFN	-1.415	-1.403	6.05
N-COF-Si-CFN	-1.687	-1.677	10.05

To elucidate the concept of the dipole moment in sensor materials, we utilized the DFT tool to gain insight into the charge separation within each system. The COF system has a negligible dipole moment (0.00 D), indicating a highly symmetric charge distribution and very low polarity. This suggests limited interactions with external fields, which might reduce sensitivity in sensor applications. In contrast, N-COF shows a significant increase in the dipole moment (0.60 D), indicating increased polarity and enhanced potential for interactions with external fields, thereby improving sensitivity. N-COF-Si, with a dipole moment of 1.32 D, demonstrates even greater polarity, suggesting further enhancement in sensor performance due to better electronic interactions. N-COF-P (1.68 D) and N-COF-S (1.83 D) exhibit the highest dipole moments before interaction, indicating the highest intrinsic polarity and potential for strong interactions with external fields, which are beneficial for sensor applications requiring high sensitivity. Furthermore, after interaction with CFN, the dipole moments increase significantly, reported as 6.05 D for N-COF-S-CFN, 7.06 D for N-COF-P-CFN, 7.29 D for COF-CFN, 9.15 D for N-COF-CFN, and 10.05 D for N-COF-Si-CFN (See **table 5**) in increasing order. The interaction with CFN notably enhances the dipole moments, suggesting a substantial increase in the molecular polarity and asymmetric charge distribution, which can significantly improve sensitivity and performance. Based on these dipole moment results, the favorable system for sensor applications appears to be N-COF-Si-CFN. This system has the highest dipole moment after interaction with CFN, indicating that it has the greatest molecular polarity and potential for strong interactions with external fields, leading to enhanced sensitivity and performance. While other systems also show significant increases in dipole moments, N-COF-Si-CFN stands out because of its pronounced polarity,

making it the most suitable for applications requiring high sensitivity and efficient charge interactions.

3.5 Visual studies

3.5.1 QTAIM analysis

For better understanding and careful investigation of the intermolecular interactions of atoms, a topological study known as the quantum theory of atoms-in-molecule (QTAM) has been employed **[65-66]**. For more knowledge about intra- and intermolecular interactions, atom-in-molecule (AIM) analysis was carried out as proposed by Richard Bader **[67-71].** it has been found that for closed-shell interactions, the values of electron density ρ(r) vary from 0.002 a u to 0.016 for van der Waal forces and 0.0024 a.u. to 0.0547 a.u. for strong electrostatic interactions **[72]**, indicating weak and strong van der Waals interactions, respectively. Herein, the obtained value for ρ(r), as computed in **Table S2**, shows an electrostatic interaction between the surface and that of the drug molecule, with extracted values ranging from 0.002- 0.009. Values in this range at critical points indicate covalent bonding with varying degrees of strength and electron sharing. The higher the value is, the stronger and more concentrated the bonding interaction. **[73]**. The result obtained from $\nabla^2\rho$ (r) indicates the strong share-shell interatomic interaction evidenced by a local concentration of the electron density distribution at the critical point when the Laplacian of the electron density $\nabla^2\rho\ (r)\ is$ less than zero **[74-75]**. going further, the literature review shows that positive values of λ_2 are an indication of steric repulsion, which destabilizes the interaction; meanwhile, negative values indicate an attractive force, which stabilizes the interaction **[76-77]**. The result obtained, λ2, has positive and negative values. Nevertheless, the negative values superseded the positive values, which is an indication of the high level of attractive force, resulting in stabilization of the adsorbent and the absorbate. From the calculated values of ρ(r), $\nabla^2\rho(r)$, V(r), G(r), E(r), and λ_2, which are summarized in **Table S2**, negative values of H(r) were observed from C_{123}--H_{25}, indicating an interaction at this point to a covalent bond, whereas other forms (H138–C28, H141-C19, and H103-H87.) had positive values of 0.10 a.u., 0.12 a.u., and 0.49 a.u., respectively, indicating strong electrostatic bonding. The density of all the electrons on the studied surface was observed to be in the following range: 0.004 to 0.009 a.u. for COF-CFN, 0.002 a.u. to 0.008 a.u. for N-COF-CFN, 0.002 a.u. to 0.009 a.u. for N-COF-P-CFN, 0.009 a.u. to 0.02 a.u.

for N-COF-S-CFN, and 0.006 a.u. to 0.01 a.u. for N-COF-Si-CFN. The different ranges in the density of electrons observed and the different topology parameters could be attributed to the presence of doped atoms on the pristine surface.

3.5.2 NCI analysis

To determine the noncovalent interactions present in the complexes, a technique known as noncovalent interaction (NCI) analysis was carried out. This analysis serves as an essential tool for determining the interaction between an adsorbate and an adsorbent. **[78].** It relies on various forms of electrostatic attraction, which are generally weaker than covalent bonds. In adsorption/sensor studies, this analysis is employed to study the interaction between the surfaces and adsorbates by checking the concentrations of different parameters, such as the hydrogen bond (force of attraction), van der Waals force (weak force of interaction), and steric repulsive force. These parameters are represented with colors: the hydrogen bond is presented in blue, the van der Waals force is represented in green, and the steric repulsive force is represented in red **[79].** Their weak forces arise from the interaction of molecular or atomic entities, driven by differences in charge distribution, rather than the sharing of electrons between atoms **[80].** The noncovalent interaction method utilizes the product of the second eigenvalue of the Hessian matrix (λ2) with the electron density ρ (sign (λ2) ρ) to analyze weak noncovalent interactions. Visualization of these weak interactions is easy through the 3D iso-surface plots presented in **Figure 3**. Specifically, the results demonstrate high localization of green iso-surfaces between the surface and the adsorbate among all the studied complexes **(**COF-CFN, N-COF-CNF, N-COF-P-CFN, N-COF-S-CFN, and N-COF-Si-CFN).), highlighting weak van der Waals interactions and confirming the excellent performance of the modified nanomaterial **[81]**. On the other hand, the presence of the red iso-surface observed at intramolecular regions of the modified surface indicates steric or strong repulsive forces. **[82]** Conclusively, the rare presence of the blue iso-surfaces shown in N-COF-Si-CFN demonstrates hydrogen bonding, which could be ascribed to the doping of silicon atoms, thereby resulting in this unique property. This result is confirmed by the second eigenvalues shown in **Table S2**, with the respective eigenvalues ranging from -0.81 to 0.97, which all lie between the hydrogen bond and the repulsive steric force of attraction, which is an indication of high van der Waals forces. However, the eigenvalue (λ2) range observed for the interacting systems demonstrated the presence of noncovalent interactions.

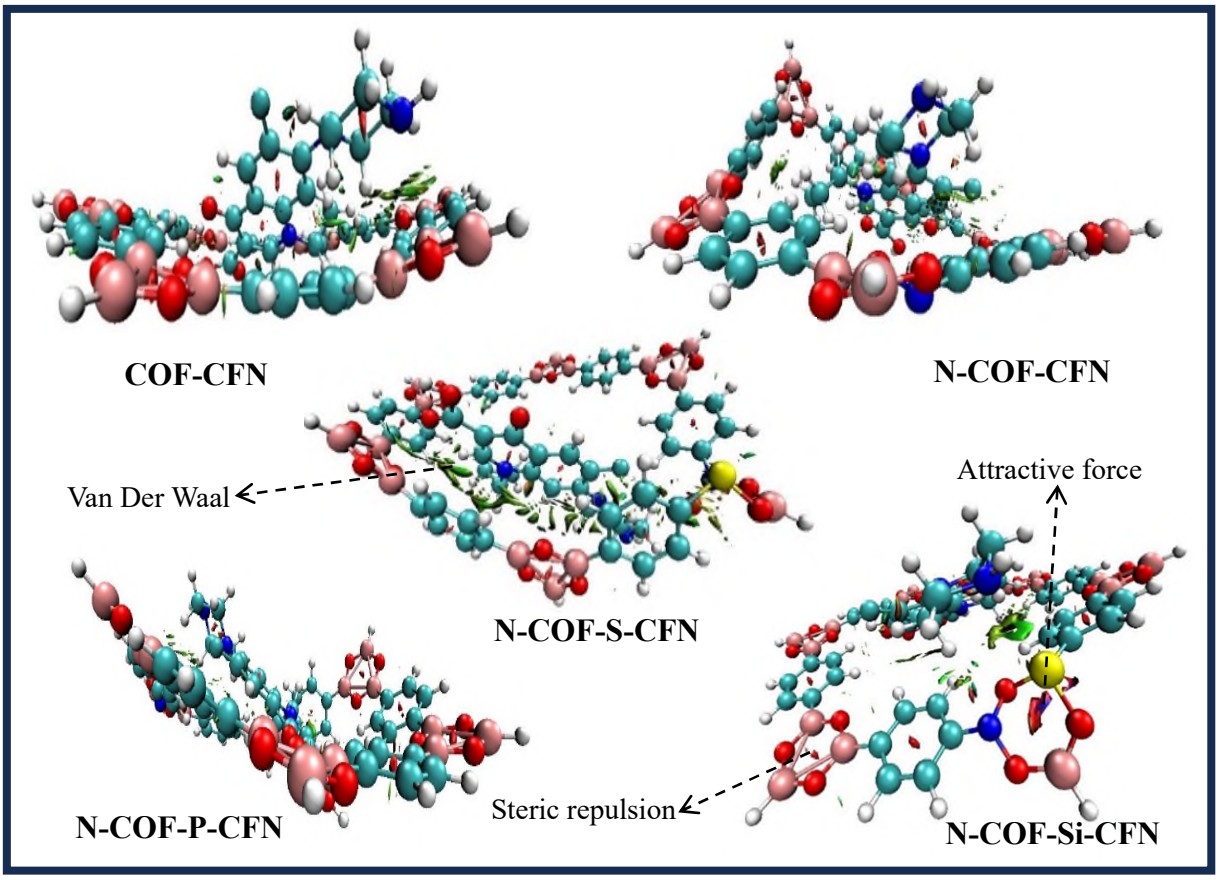


Figure 3. 3D illustration of non-covalent interaction

4.0 Conclusion

This research investigated the adsorption capacity of covalent organic frameworks (COFs) doped with heteroatoms such as nitrogen, phosphorus, sulfur, and silicon to enhance their ability to absorb ciprofloxacin. Using density functional theory (DFT) with the ωB97XD/6-311G(d) level of theory, the structures were optimized, and the electronic properties of these modified COFs were evaluated. The study of structural analysis revealed stability among the systems, with most of the systems retaining similar bond lengths after adsorbing CFN. However, the studied systems exhibit similar increases in bond lengths before and after interactions, except for system N-COF-CFN, which exhibits a decrease in bond length, implying the high conductivity and selectivity of the system with the CFN. The energy gap between the HOMO-LUMO level for the surfaces, COF (8.816 eV), N-COF (8.205 eV), N-COF-S (7.315 eV), N-COF-P (8.207 eV), and N-COF-Si (7.284 eV), decreased appreciably after interacting with CFN, suggesting that these surfaces have promising reactivity against CFN. The NBO results indicate that the COF-CFN system has strong LP $\rightarrow \sigma^*$ interactions with $E^{(2)}$ values of approximately 100-108 kcal/mol and significant F(ij) values. The N-COF-CFN system exhibits both LP $\rightarrow \sigma^*$ and $\pi^* \rightarrow \pi^*$ interactions, with the latter showing exceptionally high $E^{(2)}$ values, indicating strong π^* interactions. The N-COF-S-CFN system displays a mix of $\pi^* \rightarrow \pi^*$ and LP $\rightarrow \sigma^*$ interactions with varying strengths. Interestingly, the adsorption energy results revealed that COFs without heteroatom doping strongly chemisorbed to ciprofloxacin, with an adsorption energy of -1.088 eV. However, doping COF with nitrogen and phosphorus reduced its adsorption capacity, as indicated by the adsorption energy of -0.354 eV for N-COF-P-CFN. Conversely, doping COFs with nitrogen alone or in combination with sulfur and silicon improved chemisorption, with adsorption energies of -1.116 eV, -1.415 eV, and -1.687 eV for N-COF-CFN, N-COF-S-CFN, and N-COF-Si-CFN, respectively. In conclusion, the methodology applied in this research emphasizes a very promising outcome from all the studies, suggesting that COFs and doping with some heteroatoms, such as N, Si, and S, could yield promising adsorption properties for CFNs. Hence, our results suggest that the engineered COF should further be subjected to experimental investigations.

5.0 Declaration

5.1 Authors' contributions

Okpanachi Oyibo Nuhu: Project conceptualization, Administration, and design. **Lubem Aondokaa**: Writing, analysis, methodology, and manuscript first draft. **Maryann A. Odume and Jovita K. Ngene**: Analysis, writing, visualization, and validation.

5.2 Conflicts of Competing Interest

All authors declare no financial or interpersonal conflicts of interest that could have influenced the research or the results reported in this paper.

5.3 Availability of data

All information regarding this study is presented in this document and the supporting information.

5.4 Ethical approval

We want to clarify that our research did not require ethical approval, and we have accordingly updated the statement to reflect this information.

5.5 Funding

No governmental or non-governmental organization provided funding for this study.

5.6 Informed consent: Not applicable

References

1. Taylor, D. & Senac, T. (2014). Human pharmaceutical products in the environment–the "problem" in perspective. *Chemosphere*, *115*, 95-99.
2. Boxall, A. B. (2004). The environmental side effects of medication: How are human and veterinary medicines in soils and water bodies affecting human and environmental health? *EMBO reports*, *5*(12), 1110-1116.
3. Samal, K., Mahapatra, S., & Ali, M. H. (2022). Pharmaceutical wastewater as Emerging Contaminants (EC): Treatment technologies, impact on environment and human health. *Energy Nexus*, *6*, 100076.
4. Daughton, C. G. (2001). Pharmaceuticals and personal care products in the environment: overarching issues and overview.
5. Kümmerer, K. (2009). The presence of pharmaceuticals in the environment due to human use–present knowledge and future challenges. *Journal of environmental management*, *90*(8), 2354-2366.
6. Velpandian, T., Halder, N., Nath, M., Das, U., Moksha, L., Gowtham, L., & Batta, S. P. (2018). Unsegregated waste disposal: an alarming threat of antimicrobials in surface and ground water sources in Delhi. *Environmental Science and Pollution Research*, *25*, 29518-29528.
7. Fick, J., Söderström, H., Lindberg, R. H., Phan, C., Tysklind, M., & Larsson, D. J. (2009). Contamination of surface, ground, and drinking water from pharmaceutical production. *Environmental Toxicology and Chemistry*, *28*(12), 2522-2527.
8. Hou, L., Fu, Y., Zhao, C., Fan, L., Hu, H., & Yin, S. (2022). Ciprofloxacin and enrofloxacin can cause reproductive toxicity via endocrine signaling pathways. *Ecotoxicology and Environmental Safety*, *244*, 114049.
9. Gauba, P., & Saxena, A. (2023). Ciprofloxacin properties, impacts, and remediation. *CABI Reviews*, (2023).
10. Du, J., Liu, Q., Pan, Y., Xu, S., Li, H., & Tang, J. (2023). The research status, potential hazards and toxicological mechanisms of fluoroquinolone antibiotics in the environment. *Antibiotics*, *12*(6), 1058.
11. Ory, J., Bricheux, G., Togola, A., Bonnet, J. L., Donnadieu-Bernard, F., Nakusi, L., ... & Traore, O. (2016). Ciprofloxacin residue and antibiotic-resistant biofilm bacteria in hospital effluent. *Environmental pollution*, *214*, 635-645.

12. Shariati, A., Arshadi, M., Khosrojerdi, M. A., Abedinzadeh, M., Ganjalishahi, M., Maleki, A., ... & Khoshnood, S. (2022). The resistance mechanisms of bacteria against ciprofloxacin and new approaches for enhancing the efficacy of this antibiotic. *Frontiers in public health*, *10*, 1025633.
13. Han, L., Cai, L., Zhang, H., Long, Z., Yu, Y., & Fang, H. (2019). Development of antibiotic resistance genes in soils with ten successive treatments of chlortetracycline and ciprofloxacin. *Environmental pollution*, *253*, 152-160.
14. Boxall, A. B. (2004). The environmental side effects of medication: How are human and veterinary medicines in soils and water bodies affecting human and environmental health?. *EMBO reports*, *5*(12), 1110-1116.
15. Sungur, Ş. (2022). Pharmaceutical and personal care products in the environment: occurrence and impact on the functioning of the ecosystem. In *Emerging Contaminants in the Environment* (pp. 137-157). Elsevier.
16. Khetan, S. K., & Collins, T. J. (2007). Human pharmaceuticals in the aquatic environment: a challenge to green chemistry. *Chemical reviews*, *107*(6), 2319-2364.
17. Néstor, M. C., & Mariana, C. (2019). Impact of pharmaceutical waste on biodiversity. *Ecopharmacovigilance: Multidisciplinary Approaches to Environmental Safety of Medicines*, 235-253.
18. Ingle, A. P., Seabra, A. B., Duran, N., & Rai, M. (2014). Nanoremediation: a new and emerging technology for the removal of toxic contaminant from environment. In Microbial biodegradation and bioremediation (pp. 233-250). Elsevier
19. Hajipour, M. J., Saei, A. A., Walker, E. D., Conley, B., Omidi, Y., Lee, K. B., & Mahmoudi, M. (2021). Nanotechnology for targeted detection and removal of bacteria: opportunities and challenges. Advanced Science, 8(21), 2100556.
20. Qu, X., Brame, J., Li, Q., & Alvarez, P. J. (2013). Nanotechnology for a safe and sustainable water supply: enabling integrated water treatment and reuse. Accounts of chemical research, 46(3), 834-843.
21. Baig, N., Kammakakam, I., &Falath, W. (2021). Nanomaterials: A review of synthesis methods, properties, recent progress, and challenges. *Materials Advances*, *2*(6), 1821-1871.

22. Nath, N. S., Bhattacharya, I., Tuck, A. G., Schlipalius, D. I., & Ebert, P. R. (2011). Mechanisms of phosphine toxicity. *Journal of toxicology*, *2011*(1), 494168.
23. Li, J. R., Kuppler, R. J., & Zhou, H. C. (2009). Selective gas adsorption and separation in metal–organic frameworks. *Chemical Society Reviews*, *38*(5), 1477-1504.
24. Wang, C., Yin, L., Zhang, L., Xiang, D., & Gao, R. (2010). Metal oxide gas sensors: sensitivity and influencing factors. *sensors*, *10*(3), 2088-2106.
25. Bhati, V. S., Kumar, M., & Banerjee, R. (2021). Gas sensing performance of 2D nanomaterials/metal oxide nanocomposites: A review. *Journal of Materials Chemistry C*, *9*(28), 8776-8808.
26. Abrahi Vahed, S., & Hemmati Tirabadi, F. (2023). Carbon nanocone as a potential adsorbent and sensor for the removal and detection of ciprofloxacin: DFT studies. *International Journal of New Chemistry*, *10*(4), 288-298.
27. Zhao, B., Gong, J., Song, B., Sang, F., Zhou, C., Zhang, C., ... & Chen, Z. (2022). Effects of activated carbon, biochar, and carbon nanotubes on the heterogeneous Fenton oxidation catalyzed by pyrite for ciprofloxacin degradation. Chemosphere, 308, 136427.
28. Ajala, O. A., Akinnawo, S. O., Bamisaye, A., Adedipe, D. T., Adesina, M. O., Okon-Akan, O. A., ... & Bello, O. S. (2023). Adsorptive removal of antibiotic pollutants from wastewater using biomass/biochar-based adsorbents. RSC advances, 13(7), 4678-4712.
29. Han, L., Khalil, A. M., Wang, J., Chen, Y., Li, F., Chang, H., ... & Zhang, S. (2021). Graphene-boron nitride composite aerogel: A high efficiency adsorbent for ciprofloxacin removal from water. *Separation and Purification Technology*, 278, 119605.
30. Martínez-Periñán, E., Martínez-Fernández, M., Segura, J. L., & Lorenzo, E. (2022). Electrochemical (bio) sensors based on covalent organic frameworks (COFs). *Sensors*, *22*(13), 4758.
31. Zhang, S., Liu, D., & Wang, G. (2022). Covalent organic frameworks for chemical and biological sensing. *Molecules*, *27*(8), 2586.
32. Mohan, B., Kumari, R., Singh, G., Singh, K., Pombeiro, A. J., Yang, X., & Ren, P. (2023). Covalent organic frameworks (COFs) and metal–organic frameworks (MOFs) as electrochemical sensors for the efficient detection of pharmaceutical residues. *Environment international*, *175*, 107928.

33. Skorjanc, T., Shetty, D., & Valant, M. (2021). Covalent organic polymers and frameworks for fluorescence-based sensors. *ACS sensors*, *6*(4), 1461-1481.
34. Slimani, Y., & Hannachi, E. (2023). Nanomaterials for Environmental Applications. In *Integrated Nanomaterials and their Applications* (pp. 349-391). Singapore: Springer Nature Singapore.
35. Hussain, M., Song, X., Shah, S., & Hao, C. (2020). TD-DFT insights into the sensing potential of the luminescent covalent organic framework for indoor pollutant formaldehyde. *Spectrochimica Acta Part A: Molecular and Biomolecular Spectroscopy*, *224*, 117432.
36. Zhu, M. W., Xu, S. Q., Wang, X. Z., Chen, Y., Dai, L., & Zhao, X. (2018). The construction of fluorescent heteropore covalent organic frameworks and their applications in spectroscopic and visual detection of trinitrophenol with high selectivity and sensitivity. *Chemical Communications*, *54*(18), 2308-2311.
37. Frisch, M. E., Trucks, G. W., Schlegel, H. B., Scuseria, G. E., Robb, M. A., Cheeseman, J. R., & Fox, D. J. (2016). Gaussian 16, revision C. 01.
38. Chai, J. D., & Head-Gordon, M. (2008). Long-range corrected hybrid density functionals with damped atom–atom dispersion corrections. *Physical Chemistry Chemical Physics*, *10*(44), 6615-6620.
39. Hammud, H. H., Yar, M., Bayach, I., & Ayub, K. (2023). Covalent Triazine Framework C6N6 as an Electrochemical Sensor for Hydrogen-Containing Industrial Pollutants. A DFT Study. *Nanomaterials*, *13*(6), 1121.
40. Lu T, Chen F. Multiwfn: a multifunctional wavefunction analyser. J Comput Chem. 2012;33(5):580–92.
41. Dennington R, Keith TA, Millam JM. GaussView 6.0. 16. Semichem Inc.: Shawnee Mission, KS, USA. 2016
42. Chemcraft, V. 1.8; Graphical Software for Visualization of Quantum Chemistry Computations.
43. Revvity Signals, ChemDraw Professional, Version 23.1.2.7, Revvity Signals Software, Inc., Waltham, MA, USA 2024
44. R.A. May, K.J. Stevenson, Software Rev. Origin 8 (2009).

45. Humphrey W, Dalke A, Schulten K. VMD: visual molecular dynamics. J Mol Graph. 1996;14(1):33–8
46. Jacquemin, D., & Adamo, C. (2011). Bond length alternation of conjugated oligomers: wave function and DFT benchmarks. *Journal of Chemical Theory and Computation*, *7*(2), 369-376.
47. Kraka, E., Setiawan, D., & Cremer, D. (2016). Re-evaluation of the bond length–bond strength rule: The stronger bond is not always the shorter bond. *Journal of Computational Chemistry*, *37*(1), 130-142.
48. Baiz, C. R., Błasiak, B., Bredenbeck, J., Cho, M., Choi, J. H., Corcelli, S. A., ... & Zanni, M. T. (2020). Vibrational spectroscopic map, vibrational spectroscopy, and intermolecular interaction. *Chemical reviews*, *120*(15), 7152-7218.
49. Dutta, A. (2017). Fourier transform infrared spectroscopy. *Spectroscopic methods for nanomaterials characterization*, 73-93.
50. Khan, S. A., Khan, S. B., Khan, L. U., Farooq, A., Akhtar, K., & Asiri, A. M. (2018). Fourier transform infrared spectroscopy: fundamentals and application in functional groups and nanomaterials characterization. *Handbook of materials characterization*, 317-344.
51. Rad, A. S. (2016). Terthiophene as a model sensor for some atmospheric gases: theoretical study. *Molecular Physics*, *114*(5), 584-591.
52. Eyo, A. E., Obadiah, G. A., Benjamin, I., Edet, U. O., Akor, F. O., Mbim, E., ... & Louis, H. (2023). Geometry optimization, impact of solvation on the spectral (FT-IR, UV, NMR) analysis, Quantum chemical parameters, and the bioactivity of feruloyltyramine as a potential anti-Lassa virus agent via molecular docking. *Chemical Physics Impact*, *7*, 100338.
53. Minsky, A., Meyer, A. Y., & Rabinovitz, M. (1985). Paratropicity and antiaromaticity: role of the homolumo energy gap. *Tetrahedron*, *41*(4), 785-791.
54. Klus, S., Nüske, F., & Peitz, S. (2022). Koopman analysis of quantum systems. *Journal of Physics A: Mathematical and Theoretical*, *55*(31), 314002.
55. Weinhold, F., Landis, C. R., & Glendening, E. D. (2016). What is NBO analysis and how is it useful?. *International reviews in physical chemistry*, *35*(3), 399-440.

56. Wen, X. D., Martin, R. L., Henderson, T. M., & Scuseria, G. E. (2013). Density functional theory studies of the electronic structure of solid-state actinide oxides. *Chemical reviews*, 113(2), 1063-1096.
57. Contreras, P., Seijas, L., & Osorio, D. (2021). TDOS quantum mechanical visual analysis for single molecules. *arXiv preprint arXiv:2105.12830*.
58. Li, J., & Zhang, R. Q. (2016). Strong orbital interaction in a weak CH-π hydrogen bonding system. *Scientific reports*, *6*(1), 22304.
59. Maurer, R. J., Ruiz, V. G., Camarillo-Cisneros, J., Liu, W., Ferri, N., Reuter, K., & Tkatchenko, A. (2016). Adsorption structures and energetics of molecules on metal surfaces: Bridging experiment and theory. *Progress in Surface Science*, *91*(2), 72-100.
60. Abild-Pedersen, F., Greeley, J., Studt, F., Rossmeisl, J., Munter, T. R., Moses, P. G., ... & Nørskov, J. K. (2007). Scaling Properties of Adsorption Energies for Hydrogen-Containing Molecules<? format?> on Transition-Metal Surfaces. *Physical review letters*, *99*(1), 016105.
61. Liu, Y. (2009). Is the free energy change of adsorption correctly calculated?. *Journal of Chemical & Engineering Data*, *54*(7), 1981-1985.
62. Itoh, T., Lee, D., Goto, T., Akamatsu, T., Izu, N., Shin, W., & Kasuga, T. (2016). Analysis of Recovery Time of Pt-, Pd-, and Au-Loaded SnO 2 Sensor Material with Nonanal as Large-Molecular-Weight Volatile Organic Compounds. *Sensors & Materials*, *28*(11).
63. Rizwan, A., Khalid, S., Iqbal, T., Masood, M. K., Ali, S. M., & Bano, N. (2024). Computational Investigation of Pure Antimonene and Antimonene/Bismuthene Heterostructure for Detecting Thermal Runaway Gases. *Sensors and Actuators A: Physical*, 115598.
64. Alaqarbeh, M. (2021). Adsorption phenomena: definition, mechanisms, and adsorption types: short review. *RHAZES: Green and Applied Chemistry*, *13*, 43-51.
65. Bader R, Nguyen-Dang TT, Tal Y (1981) A topological theory of molecular structure. Rep Prog Phys 44:893
66. Bader RF (1985) Atoms in molecules. Acc Chem Res 18:9–15
67. Bader RF (1991) A quantum theory of molecular structure and its applications. Chem Rev 91:893–928

68. Bader RF, Matta CF (2013) Atoms in molecules as non-overlapping, bounded, space-filling open quantum systems. Found Chem 15:253–276
69. Cortés-Guzmán F, Bader RF (2005) Complementarity of QTAIM and MO theory in the study of bonding in donor–acceptor complexes. Coord Chem Rev 249:633–662
70. Bader, R. F. W. (1990). Atoms in Molecules: A Quantum Theory. *Oxford University Press.*
71. Popelier, P. L. A. (2011). Atoms in Molecules: An Introduction*. Prentice Hall.*
72. Espinosa, E., Molins, E., & Lecomte, C. (1998*). Hydrogen bond strengths revealed by topological analyses of experimentally observed electron densities. Chemical Physics Letters,* 285(3-4), 170-173.
73. Gatti, C. (2005*). Chemical bonding in crystals: New directions. Zeitschrift für Kristallographie-Crystalline Materials,* 220(5-6), 399-457.
74. Macchi, P., & Sironi, A. (2003). *Chemical bonding in crystals: New directions. Coordination Chemistry Reviews,* 238, 383-412.
75. Bondi, A. (1964). *van der Waals volumes and radii. Journal of Physical Chemistry,* 68(3), 441-451.
76. Murray, J. S., & Sen, K. (2009). *Molecular Electrostatic Potentials: Concepts and Applications. Elsevier.*
77. Zhang, Q., Li, J., & Zhang, G. (2020). Advances in noncovalent interactions for the development of high-performance sensors. *Sensors and Actuators B: Chemical*, 310, 127818.
78. Kumar, A., & Subramaniam, C. (2021). Visualizing noncovalent interactions in sensors: A computational approach. *Journal of Physical Chemistry B,* 125(7), 1800-1810. https://doi.org/10.1021/acs.jpcb.0c09360
79. Singla, P., & Mittal, M. (2022). Mechanisms of noncovalent interactions: From molecular recognition to sensor design. *Chemical Reviews*, 122(3), 1592-1631
80. Oliveira, T. M., & Costa, R. D. (2021). Computational studies on weak noncovalent interactions in modified nanomaterials for sensor applications. *Journal of Molecular Modeling,* 27(5), 116
81. Patel, K., & Kumar, A. (2020). Understanding the role of noncovalent interactions in sensor material performance. *ACS Applied Materials & Interfaces,* 12(34), 38009-38020. https://doi.org/10.1021/acsami.0c11672

82. Dash, B., Dash, B., & Rath, S. S. (2020). A thorough understanding of the adsorption of Ni (II), Cd (II) and Zn (II) on goethite using experiments and molecular dynamics simulation. *Separation and Purification Technology*, *240*, 116649.

Supplementary Files

This is a list of supplementary files associated with this preprint. Click to download.

- CFNSupportinginformation.docx